IOPscience

Atomic and magnetic ordering in bcc Cu–Al–Mn: computational study

Atomic and magnetic ordering in bcc Cu–Al–Mn: computational study

Alejandro Alés[1] and Fernando Lanzini[1,2]

[1] Instituto de Física de Materiales Tandil (IFIMAT) and Universidad Nacional del Centro de la Provincia de Buenos Aires. Pinto 399 (7000), Tandil, Argentina
[2] CIFICEN-CONICET, Pinto 399(7000), Tandil, Argentina

E-mail: flanzini@exa.unicen.edu.ar

Abstract

The β phase of the ternary alloy Cu–Al–Mn, with bcc structure, displays an interesting variety of long-range atomic ordering and magnetic transitions. In this work, we present a model that allows an accurate reproduction of the measured critical temperatures for alloys with compositions along the pseudobinary line $Cu_3Al \leftrightarrow Cu_2AlMn$. The method is based on the Monte Carlo technique, allowing simultaneous evolution of the atomic distribution and the magnetic state. The configurational part of the energy is represented with a three-state Hamiltonian; the six interchange energies that govern the chemical interactions between nearest and next-nearest neighbours atoms have been determined. The magnetic counterpart is modelled by means of an Ising model. The predicted Curie temperatures agree well with the experimental values when it is assumed that the crystal configuration remains fixed and with the maximum possible degree of atomic ordering. The effects of configurational disorder on the magnetic transition have been evaluated.

Keywords: Cu–Al–Mn, atomic ordering, magnetism, Monte Carlo simulations

(Some figures may appear in colour only in the online journal)

1. Introduction

The ternary alloy Cu–Al–Mn belongs to a family of Cu-based alloys (Cu–Zn–Al, Cu–Al–Be, Cu–Al–Ni) which present, under certain conditions, a martensitic transformation. This is a diffusionless solid-to-solid transition: by means of small cooperative atomic displacements, the material changes its structure and crystallographic orientation. The technological interest in the alloys that display this kind of transformation is connected to the presence of certain
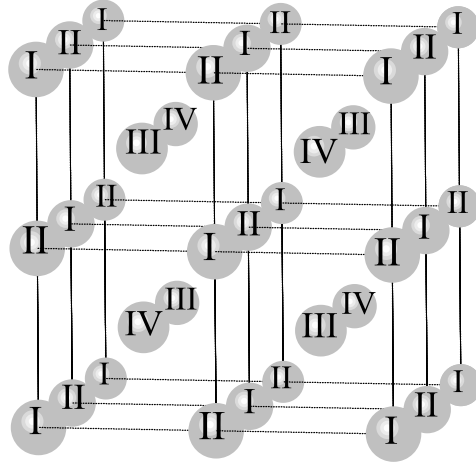
Figure 1. The general bcc lattice and the four interpenetrating fcc sublattices in which it is subdivided.

thermomechanical properties such as shape memory effect, pseudoelasticity and high damping capacity [1–4].

Owing to the diffusionless character of the martensitic transformation, the low-temperature phase (martensite) inherits the atomic distribution of the high-temperature phase (austenite). The atomic distribution present in the parent phase affects the properties of the transformation and the resulting martensitic structure. In the Cu-based alloys, the austenitic β phase displays a more or less complex sequence of long-range ordered (*lro*) configurations, derived from a *bcc* primitive lattice. The study of the type and degree of atomic order at given conditions of temperature and composition has interest from both the fundamental and the applied points of view.

The typical ordered structures occurring in this system are shown in figure 1. The bcc primitive lattice is subdivided into four interpenetrating fcc sublattices, I–IV, and the occupation probabilities p_i^α for an atom of type i (i = Cu, Mn or Al) in the αth lattice (α = I–IV) are defined. The disordered (or short-range ordered) A2 configuration is characterized by the relation,

$$p_i^{\mathrm{I}} = p_i^{\mathrm{II}} = p_i^{\mathrm{III}} = p_i^{\mathrm{IV}} = c_i, \tag{1a}$$

with c_i the atomic fraction of the ith element.

A structure with order in nearest neighbours, B2, is often present at intermediate temperatures. The B2 configuration is defined by

$$p_i^{\mathrm{I}} = p_i^{\mathrm{II}} \neq p_i^{\mathrm{III}} = p_i^{\mathrm{IV}}. \tag{1b}$$

Other usual configurations, ordered both in nearest and next-nearest neighbours, are DO$_3$, with an atomic distribution given by

$$p_i^{\mathrm{I}} = p_i^{\mathrm{II}} = p_i^{\mathrm{III}} \neq p_i^{\mathrm{IV}}, \tag{1c}$$

and L2$_1$,

$$p_i^{\mathrm{I}} = p_i^{\mathrm{II}} \neq p_i^{\mathrm{III}} \neq p_i^{\mathrm{IV}}. \tag{1d}$$

A number of experimental studies about long-range ordering transitions in β Cu–Al–Mn have been carried out in the past [5–9]. Most of this research has been devoted to the pseudobinary line of compositions Cu$_3$Al $\leftrightarrow$ Cu$_2$AlMn [5, 6], although alloys with compositions belonging

to the lines $Cu_3Al \leftrightarrow Cu_3Mn_2$ [8, 9], $Cu_3Al \leftrightarrow Mn$ [9] have also been studied. Kainuma *et al* [7] measured the critical temperatures for a great number of compositions, mostly corresponding to fixed Al atomic percentages of 10%, 15% and 20%.

Despite this considerable amount of experimental information, a clear picture of the phase diagram is still lacking. Whereas it is well established that the alloys richer in Mn (say, with $c_{Mn} > 10$ at%) experience a two-step ordering process A2 $\leftrightarrow$ B2 $\leftrightarrow$ L2$_1$, as the Mn content is reduced the situation becomes less clear. In some works, a double transition is also proposed for alloys with very low Mn content [6–8], and even for the limiting binary Cu–Al. However, studies on Cu–Al [10], and diluted ternary Cu–Al–*X* systems [9,11–13] indicate that, in both cases, there is a single A2 $\leftrightarrow$ DO$_3$ (L2$_1$) transformation. This conflict can be attributed, primarily, to the complications associated with the experimental assessment of this region of the phase diagram. For instance, in Cu–Al, the ordering of the β phase takes place at temperatures at which it is unstable against decomposition into the equilibrium α (fcc) and γ (complex cubic) phases [10, 14]. The measured ordering temperature in Cu$_3$Al is around 810 K, but its lower stability limit is 840 K [15]. Thus, measurements of the ordering reactions require very careful experimental procedures and detailed analysis.

Since most of the evidence indicates that in Cu–Al the *lro* is established by a single reaction A2 $\leftrightarrow$ DO$_3$, while it is clear that for ternary alloys with a considerable amount of Mn the ordering occurs in two steps A2 $\leftrightarrow$ B2 $\leftrightarrow$ L2$_1$, an interesting question that arises is about the Mn content at which the splitting from one to two ordering transitions takes place.

A feature that distinguishes Cu–Al–Mn from other Cu-based shape memory alloys is the existence of magnetic properties. Magnetism originates at the Mn atoms, which have a localized magnetic moment of $\sim 4 \mu_B$ [16, 17]. The stoichiometric Cu$_2$AlMn (Heusler alloy) is ferromagnetic, with a relatively high Curie temperature of ~ 630 K [18]. It has been suggested that the magneto-crystalline coupling can lead to the magnetic control of the shape-memory effect [19, 20].

This work has several objectives. Firstly, we present a model able to reproduce the chemical ordering temperatures for alloys with compositions along the pseudobinary line Cu$_3$Al $\leftrightarrow$ Cu$_2$AlMn. The model is based on a set of pairwise interactions (interchange energies) in nearest and next-nearest neighbours, whose values are determined by fitting to experimental data. Although other authors have previously made efforts in this direction [8, 9], we follow here a different approach, whose advantages will be discussed below. The thermal evolution of the atomic configuration is studied by means of Monte Carlo simulations based on the Blume–Emery–Griffiths model [21]. Secondly, we present a simple model to describe the magnetic ordering temperatures in alloys with compositions close to Cu$_2$AlMn. Numerical values for the magnetic exchange integrals in first and second neighbours of the Mn fcc sublattice are determined, combining results of *ab initio* calculations and experimental data. The model allows a satisfactory reproduction of the experimental Curie temperatures. Finally, we analyse the interplay between chemical and magnetic ordering.

This paper is organized as follows. In section 2 we describe the implementation of the numerical methods. In section 3 the result of our calculations are presented and discussed, and in section 4 the main conclusions are outlined.

2. Methods

2.1. Monte Carlo simulations

The Monte Carlo method [22, 23] is based on the simulation of the alloy configuration in a computational crystal. This is one of the most powerful methods for the study of

thermodynamical properties in alloys [24, 25]. This technique allows obtaining 'quasi-exact' information [25] about several properties associated with the alloy configuration.

In the present work, simulations were performed on virtual crystals comprising $N = 2 \times 32^3$ sites under periodic boundary conditions. The sites in the box were sequentially visited; at every site the possibility of inverting the magnetic moment and/or interchanging the local atom with one of their nearest neighbours was evaluated. At each temperature, a minimum of 5×10^4 Monte Carlo steps (interchange attempts per atom) were performed, in order to ensure thermal equilibration. A few additional runs with random selection of the visited sites were made; the results perfectly agree with the ones obtained within the sequential procedure. This test allows concluding that no undesirable correlations effects are introduced by the method used in this work.

In order to simulate the atomic occupation, a variable σ_i was associated to each site i in the lattice, $\sigma_i = +1, 0$ or -1, depending on whether the site i was occupied by a Cu, Mn or Al atom, respectively. The evolution of the atomic configuration was simulated by considering the direct interchange between a given atom and one of their eight nearest neighbours, chosen at random. The probability of interchange obeyed the Metropolis criterion [26]:

$$p_{\text{int}} = \min\left\{1, \ \exp\left(-\Delta H_{\text{conf}}/k_B T\right)\right\},$$

where k_B is the Boltzmann constant, T the absolute temperature and the difference in configurational energy, ΔH_{conf}, was calculated by means of the Blume–Emery–Griffiths (BEG) Hamiltonian [21]:

$$H_{\text{conf}} = \sum_s \sum_{<ij>} \left\{ J_s \sigma_i \sigma_j + K_s \sigma_i^2 \sigma_j^2 + L_s \left(\sigma_i^2 \sigma_j + \sigma_i \sigma_j^2\right)\right\}. \tag{2}$$

In the preceding expression, the index s refers to the sth coordination sphere; all the pairs $<ij>$ placed as sth neighbours are included in the summation. As is usual in the treatment of this family of alloys, only chemical interactions between nearest ($s = 1$), and next nearest neighbours ($s = 2$) were included in the model; the interactions between more distant pairs were assumed to be zero.

The parameters J_s, K_s and L_s in equation (2) are defined as

$$J_s = \frac{1}{4} W_{\text{CuMn}}^{(s)}, \quad K_s = \frac{1}{4}\left(2 W_{\text{CuAl}}^{(s)} + 2 W_{\text{MnAl}}^{(s)} - W_{\text{CuMn}}^{(s)}\right), \quad L_s = \frac{1}{4}\left(W_{\text{CuAl}}^{(s)} - W_{\text{MnAl}}^{(s)}\right),$$

$$\tag{3}$$

where $W_{\text{AB}}^{(s)} = -2 V_{\text{AB}}^{(s)} + V_{\text{AA}}^{(s)} + V_{\text{BB}}^{(s)}$ are the interchange energies for A and B atoms placed as sth neighbours, being $V_{\text{AB}}^{(s)}$ the corresponding interatomic potential. The interchange energies $W_{\text{AB}}^{(s)}$ are the quantities that ultimately determine the crystalline behaviour of the alloy: positive values imply ordering tendency, and negative ones lead to segregation.

In order to simulate the magnetic configuration of the alloy, a second variable S_i was assigned to each site i in the lattice. This variable represents the magnetic state of the atom placed at i, and can take one of the values $S_i = \pm S$ or 0. For the non-magnetic elements Cu and Al, $S_i = 0$, whereas for the Mn atoms S_i took the values $+S$ or $-S$. The simulation of the magnetic evolution was performed by evaluating, at each Mn site, the probability of performing a spin flip $S_i \rightarrow -S_i$. As above, this probability was given by the Metropolis

formula,

$$p_{\text{flip}} = \min \left\{ 1, \ \exp \left(-\Delta H_{\text{magn}} / k_{\text{B}} T \right) \right\},$$

with ΔH_{magn} given by the Ising model

$$H_{\text{magn}} = - \sum_s \sum_{\langle ij \rangle} J_s^M S_i S_j. \tag{4}$$

Here, J_s^M is the magnetic coupling between the magnetic atoms placed as sth neighbours.

Three kinds of simulations were performed. First, a series of simulations analysing the evolution of configurational order and ignoring the magnetic interactions was made. The critical temperatures obtained in the simulations were fitted to the experimental values; in this way, a set of six interchange chemical energies $W_{\text{AB}}^{(s)}$ ($s = 1, 2$) was determined. Secondly, we performed simulations of the magnetic ordering on lattices with fixed atomic arrangement. It was assumed that the distribution corresponded to the maximum degree of atomic order attainable for each composition. Finally, simulations in which both the atomic and magnetic configurations were free to evolve were done. At each atomic site, the possibility of inversion of the magnetic moment was first evaluated and the interchange with a neighbouring site was considered next.

2.2. First principles calculations

Electronic structure calculations based on the density functional theory (DFT) [27] were carried out using the pseudopotential method and a plane wave basis set. The calculations have been performed within the Quantum Espresso 5.0.2 code [28]. The interactions of the atomic core and the valence electrons were described by ultrasoft pseudopotentials [29]. The exchange-correlation term was approximated by spin-polarized generalized gradient approximation (GGA) according to the Perdew–Burke–Ernzerhof (PBE) parametrization [30]. The plane-wave basis cut-off energy was set to 40 Ry (400 Ry for the electronic density). Brillouin zone integration was performed with a $10 \times 10 \times 10$ k-point grid automatically generated following the convention of Monkhorst and Pack [31]. The convergence threshold for the electronic energy was set to 10^{-5} Ry.

3. Results and discussion

3.1. Atomic ordering

3.1.1. Determination of the interchange energies. The first objective of the present work was the determination of a set of chemical interchange energies $W_{\text{AB}}^{(s)}$ that allows the reproduction of the experimental order–disorder temperatures. As stated above, and as is usual in studies of ordering in Cu-based shape memory alloys [8, 9, 11, 13, 32–35], the model includes only pairwise interactions between nearest and next-nearest neighbours. Neither interactions between more distant pairs nor multi-body terms have been taken into consideration.

Other authors have previously proposed numerical values for the interchange energies. Prado *et al* [8] fitted experimental order–disorder temperatures using analytical expressions within a modified Bragg–Williams–Gorski (BWG) model [36]. The values obtained for the interchange energies are detailed in table 1. It should be noted that these authors assumed a double ordering transition even in the limiting binary Cu_3Al. Later, Obradó *et al* [9] fitted the experimental data from [5] for alloys with compositions along the line $Cu_3Al \leftrightarrow Cu_2AlMn$. These authors used an inverse Monte Carlo scheme based on a simplified version of the BEG Hamiltonian, equation (2). In order to reduce the number of adjustable parameters, they

Table 1. Pair interchange energies proposed for other authors and those obtained in the present work. Units are kelvin degrees; the numerical values are obtained dividing the interchange energies by the Boltzmann constant.

$W_{CuAl}^{(1)}$ (K)	$W_{CuAl}^{(5)}$ (K)	$W_{CuMn}^{(1)}$ (K)	$W_{CuMn}^{(5)}$ (K)	$W_{MnAl}^{(1)}$ (K)	$W_{MnAl}^{(5)}$ (K)	Reference
1605	856	1266	353	2144	1168	[8]
1552	1008	388	−175	388	679	[9]
1660	920	600	200	700	800	This work

imposed three arbitrary restrictions to the interchange energies, by taking K_1, K_2 and L_1 in equation (3) equal to zero.

In the present work we have determined a new set of nearest and next-nearest neighbours energies following a procedure similar to that used in [9]—i.e. an inverse Monte Carlo scheme—although with some remarkable differences. First, it should be noted that the number of adjustable parameters (six) is relatively high. In order to reduce the number of parameters without resorting to unphysical simplifications, we have taken advantage of the fact that the interchange energies for Cu–Al pairs are well known. Their values have been estimated by several authors, using different analytical or numerical methods and data from different ternary Cu–Al–X systems [8, 9, 11, 13,32–35]. The calculated values range from 1030 K to 1660 K for $W_{CuAl}^{(1)}$, and from 540 K to 1008 K for $W_{CuAl}^{(5)}$; usually, the mean field (BWG) approximation gives lower estimates than more elaborate methods. Although the range of published values is considerable, the general agreement indicates that the interchange energies are not only parameters of a given model or alloy system, but they also have a physical meaning [9]. Particularly, it has been shown in [37] that the values proposed in [13] to model the transition temperatures in Cu–Al–Zn, also satisfactorily reproduces the topology of the A2 + DO$_3$ two-phase field in Cu–Al. Therefore, we have taken for the Cu–Al interchange energies the values calculated in [13]: $W_{CuAl}^{(1)} = 1660$ K and $W_{CuAl}^{(5)} = 920$ K.

The four remaining unknowns were determined by an iterative procedure of successive approximations, fitting alternately the experimental transition temperatures $T_{A2\leftrightarrow B2}$ and $T_{B2\leftrightarrow L2_1}$ of alloys with compositions along the line Cu$_3$Al $\leftrightarrow$ Cu$_2$AlMn. The obtained results are listed in table 1. It is evident that, whereas the interchange energies for the Cu–Al pairs are consistent with the results of other authors, the values for Cu–Mn and Mn–Al differ significantly. This could be attributed to the uncertainty in the experimental data and the use of different theoretical approaches.

3.1.2. Atomic ordering temperatures.

Line Cu$_3$Al $\leftrightarrow$ Cu$_2$AlMn. The calculated critical temperatures for atomic ordering are displayed in figure 2, and compared with experimental values from [5, 7, 13]. The critical temperatures were determined by analysing the thermal evolution of the long-range ordered parameters defined below and shown in figure 3. According with the discussion in section 1, we discarded, from [7], the experimental data corresponding to Mn contents below 10 at%. The calculated results closely agree with the experimental ones for compositions close to Cu$_3$Al and Cu$_2$AlMn. At intermediate compositions $T_{A2\leftrightarrow B2}$ seems to be slightly underestimated by the simulations; we understand, however, that more experimental information in this region of the phase diagram is needed in order to draw a definitive conclusion.
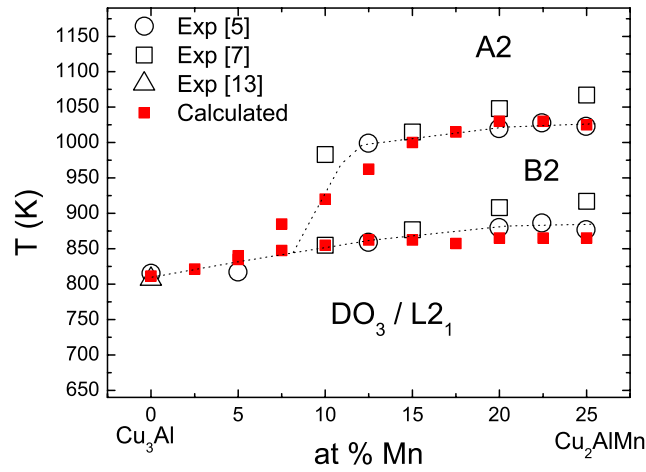
Figure 2. Experimental and calculated ordering temperatures along the pseudobinary line Cu₃Al ↔ Cu₂AlMn. Lines through the experimental data are just guides to the eye.
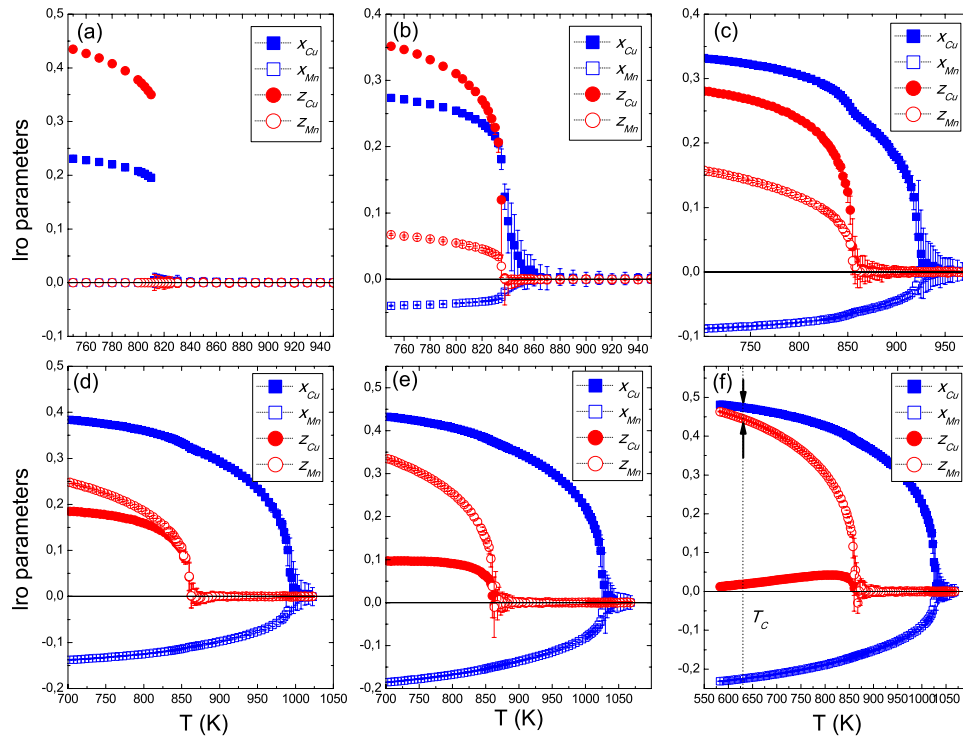
Figure 3. Thermal evolution of the long-range order for six alloys with compositions along the line Cu₃Al↔Cu₂AlMn (fixed 25 at% Al): (*a*) Cu₃Al; (*b*) 5 at% Mn; (*c*) 10 at% Mn; (*d*) 15 at% Mn; (*e*) 20 at% Mn; (*f*) Cu₂AlMn. Note the different horizontal and vertical scales.

The compositions represented in figure 3 correspond to a fixed content of 25% at Al, from Cu_3Al (figure 3(a)) to Cu_2AlMn (figure 3(b)). It can be appreciated the way in which the number and nature of ordering transitions change as the copper atoms are replaced with manganese. In the binary Cu_3Al, there is single transition, from the A2 configuration towards a structure ordered in first and second neighbours, DO_3. The same occurs for an alloy with 2.5 at% Mn. For 5% at. Mn (figure 3(b)), the transition splits into two reactions taking place at close temperatures: the ordering to a B2 configuration is followed, a few degrees below, by the ordering of next-nearest neighbours giving rise to an $L2_1$ superlattice. Further increasing the Mn content up to 15 at%, $T_{A2 \leftrightarrow B2}$ smoothly increases, while $T_{B2 \leftrightarrow L2_1}$ remains almost unchanged (figures 3(c)–(d)). Finally, above 15 at% Mn, both $T_{A2 \leftrightarrow B2}$ and $T_{B2 \leftrightarrow L2_1}$ show little variation with composition.

Figure 3 also shows the different kinetic nature of the transitions. On the one hand, the single ordering reaction arising for alloys with low Mn content is accompanied by a sudden change in the order parameters. This agrees with the observed first-order character of the reaction [9, 11, 13]. Instead, below the A2 $\leftrightarrow$ B2 transition in alloys with high Mn content, the *lro* parameters increase smoothly from zero, in accordance with the experimental observation that this is a continuous transition. Also the B2 $\leftrightarrow$ $L2_1$ transition shows a continuous character. The values of the order parameters quantify the atomic distribution on the lattice sites. In particular, it should be noted that both next-nearest neighbours parameters, z_{Cu} and z_{Mn}, take positive values in the $L2_1$ configuration. It means that the preferred low-temperature configuration is one in which Cu atoms occupy sublattices I and II (since $x_{Cu} > 0$ and grows as the temperature decreases), the remaining Cu and Mn occupy sublattice III (z_{Cu} and z_{Mn} positives) and sublattice IV is occupied by the Al atoms. The atypical thermal variation of z_{Cu} in Cu_2AlMn (figure 3(f)) can be explained as follows: below $T_{A2 \leftrightarrow B2}$ and above $T_{B2 \leftrightarrow L2_1}$ the order B2 is still incomplete and the antisite Cu atoms distribute equally between sublattices III and IV, and then $z_{Cu} = 0$. Below $T_{B2 \leftrightarrow L2_1}$ order in next-nearest neighbours is developed: Mn and Al atoms tend to accommodate in sublattices III and IV, respectively. The antisite Cu atoms occupy some of the sites of the Mn sublattice, resulting in $z_{Cu} > 0$. As the temperature further decreases, order in nearest neighbours gradually increases, and the Cu atoms placed in the Mn sublattice migrate to the Cu-sublattices I and II, and then $z_{Cu} \rightarrow 0$.

Other lines of composition. The set of interchange energies proposed in table 1 has been determined by fitting to the experimental order–disorder transition temperatures for compositions along the line connecting Cu_3Al and Cu_2AlMn. This is the most extensively studied region of the phase diagram for several reasons. Besides being particularly interesting because it includes the Heusler alloy, in this line of compositions the electronic concentration takes the fixed value $e/a = 1.5$. At this value of e/a, the bcc β phase (or the ordered superstructures derived from it) displays its maximum range of thermal stability against other competing phases such as α (fcc), and γ (complex cubic) [38–40].

There are, however, experimental assessments of other regions of the phase diagram. In figure 4, the critical temperatures predicted by our model are contrasted with experimental data taken from [9], corresponding to compositions belonging to the lines $Cu_3Al \leftrightarrow Mn$ (figure 4(a)) and $Cu_3Al \leftrightarrow Cu_3Mn_2$ (figure 4(b)).

The model captures the main characteristics of the phase diagram for these two pseudobinary lines (for instance, correctly predict the nature of the involved phases and the point where the splitting from one to two transitions takes place). However, there are some quantitative discrepancies regarding the values of the critical temperatures, being the most notorious the underestimation of $T_{A2 \leftrightarrow B2}$ for compositions along the line $Cu_3Al \leftrightarrow Cu_3Mn_2$ (figure 4(b)). A different set of interchange energies could be proposed, which improves the

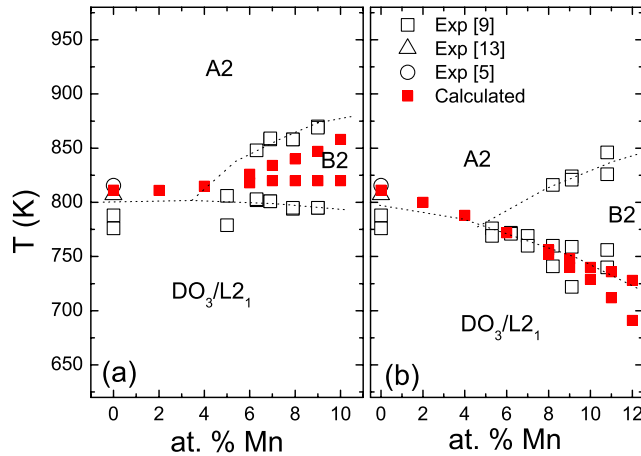**Figure 4.** Experimental and calculated order–disorder transition temperatures for alloys with compositions along the lines (*a*) $Cu_3Al \leftrightarrow Mn$; (*b*) $Cu_3Al \leftrightarrow Cu_3Mn_2$. Dotted lines through the experimental data are guides to the eye.

agreement between experiment and theory for the data displayed in figure 4; this leads, however, to a wrong prediction of the critical temperatures in the $Cu_3Al \leftrightarrow Cu_2AlMn$ line. The present results indicate that a model considering only constant interactions up to second neighbours is unable to account for the critical ordering temperatures in all the range of compositions experimentally investigated.

3.2. Magnetic ordering

3.2.1. Determination of the exchange integrals. As discussed in the Introduction to this work, besides configurational atomic ordering, β Cu–Al–Mn also shows magnetic ordering phenomena. The stoichiometric Cu_2AlMn displays a paramagnetic to ferromagnetic transition at a Curie temperature of about 630 K. The magnetism is originated by the magnetic moments localized at the Mn atoms. The localized character of the magnetic moments allows us to treat the system by means of a Heisenberg-like model [16]. In this work we have chosen, as a first approximation, a two-states Ising Hamiltonian; this model has been extensively employed by other authors to treat magnetism in Cu–Al–Mn [41–43]. The magnetic moments interact through an RKKY [41, 42] type interaction. This model [44] predicts an oscillatory and decreasing variation of the magnetic exchange integrals J_s^M with the interatomic distance, resulting in a competence between ferromagnetic and antiferromagnetic alignment tendencies. Although the J_s^M extend to considerable distances, the biggest values, corresponding to the first coordination spheres, determine the main magnetic properties of the material, in particular its Curie temperature T_C [45]. In Cu_2AlMn with perfect $L2_1$ order, the Mn atoms completely fill one of the four fcc sublattices shown in figure 1. Closest Mn–Mn pairs (nearest and next-nearest neighbours in the fcc sublattice) correspond to third and sixth neighbours of the primitive bcc lattice. Thus, for the application of the magnetic Hamiltonian of equation (4), we restricted our consideration to the terms containing J_3^M and J_6^M; the remaining exchange integrals were assumed to be zero. This is a reasonable assumption provided that the effects related to imperfect order or deviations from the stoichiometry are not significative. For instance, in Cu_2AlMn the Curie temperature T_C is considerably below the critical $T_{B2 \leftrightarrow L2_1}$ temperature.
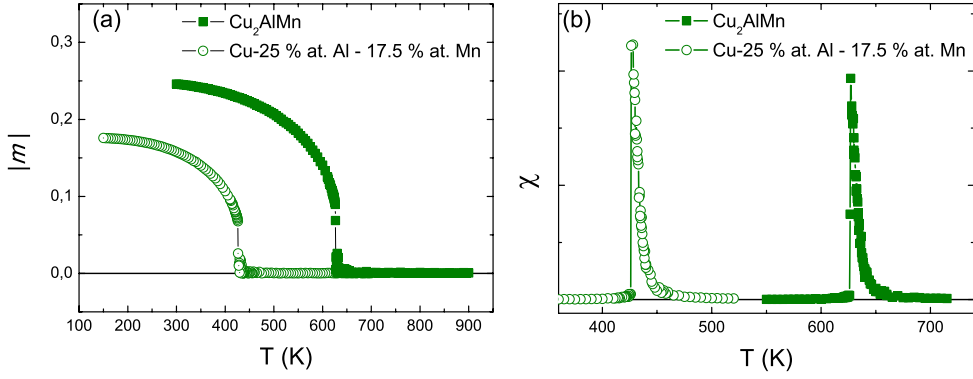
Figure 5. Evolution with temperature of (a) modulus of the normalized magnetization, $|m|$, and (b) magnetic susceptibility χ for two alloys with compositions along the line $Cu_3Al \leftrightarrow Cu_2AlMn$.

As can be seen in figure 3(f), although the crystalline ordering is not fully established at T_C, the deviation from perfect order is small. Besides, since we restrict our analysis to alloys whose Mn content is lower than 25 at%, the effects of off-stoichiometry are irrelevant provided there is a high degree of crystalline order at the temperatures at which magnetic ordering takes place. The same reasoning does not apply to alloys whose Mn content exceeds 25 at%, since in this case there is always some number of Mn antisites.

The values for J_3^M and J_6^M were estimated as follows. According to the mean field theory, the Curie temperature for the stoichiometric, perfectly ordered, alloy is given by [45–47]:

$$k_B T_C = \frac{2S(S+1)}{3}(12J_3^M + 6J_6^M),\tag{5}$$

with S the magnetic moment. On the other hand, the difference of the ground state energies for $L2_1$ Cu_2AlMn with ferromagnetic (FM) and antiferromagnetic (AFM) magnetic configurations is given by [45]

$$\Delta E = E_{FM} - E_{AFM} = -8S^2 J_3^M.\tag{6}$$

The values for ΔE and S were obtained from *ab initio* calculations, with the procedure detailed in section 2.2. The values $\Delta E = -31.55$ meV and $S = 3.63\mu_B$ were obtained. The experimental Curie temperature for Cu_2AlMn, $T_C = 630$ K, was used. Equations (5) and (6) lead to $J_3^M = 0.299$ meV and $J_6^M = 0.210$ meV. These values are comparable with the ones reported in [45] ($J_3^M = 0.333$ meV and $J_6^M = 0.329$ meV), which lead to an overestimation of the Curie temperature.

Magnetic ordering temperatures. The calculated evolution of the magnetization m and the magnetic susceptibility χ are shown in figure 5 for two alloys with compositions belonging to the line $Cu_3Al \leftrightarrow Cu_2AlMn$. Simulations were carried out assuming that the atomic distribution corresponds to the maximum possible degree of $L2_1$ order: in the stoichiometric alloy one of the fcc sublattices is fully occupied by Mn atoms. In the off-stoichiometric case (with $c_{Mn} < 25$ at%) the remaining sites of the Mn sublattice where occupied with randomly distributed Cu atoms. In figure 5, the normalized magnetization is defined as $m = (N_\uparrow - N_\downarrow)/N$, being $N_{\uparrow(\downarrow)}$ the number of magnetic atoms in the majority (minority) orientation, and N the total number of sites in the simulation lattice. With this definition, the saturation value is $m_{max} = c_{Mn}$. The paramagnetic state is characterized by a net magnetization
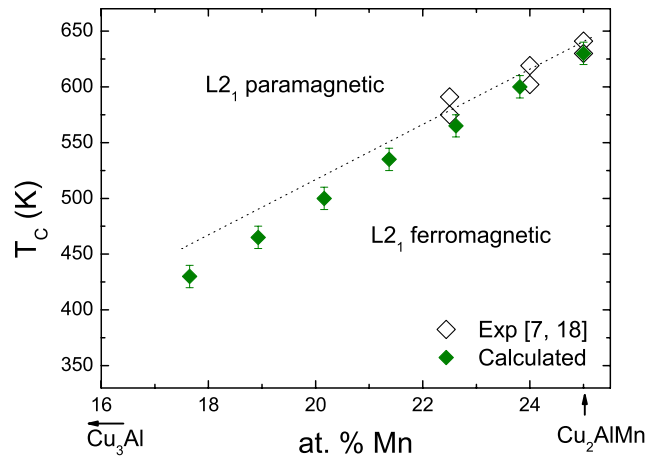
Figure 6. Measured and calculated Curie temperatures for alloys with compositions along the line Cu$_3$Al $\leftrightarrow$ Cu$_2$AlMn.

$m = 0$, whereas in the ferromagnetic state it is $m \neq 0$; the Curie temperature is located at the transition between these states. The temperature of the magnetic transformation can be determined from the plot of the magnetic susceptibility (figure 5(b)). This is obtained from the magnetization fluctuations as $\chi = \frac{1}{k_B T^2}\left[\langle m^2\rangle - \langle m\rangle^2\right]$.

The temperatures of magnetic ordering for a series of alloys Cu–Al–Mn with compositions close to Cu$_2$AlMn have been experimentally determined in [7]. The results of those experiments are shown in figure 6, and compared with the predictions of the present model. There is a good agreement between measured and calculated critical temperatures: T_C grows linearly with the Mn content.

3.3. Simultaneous atomic and magnetic ordering

In this section, the interplay between chemical and magnetic ordering is analysed. A new series of simulations was performed, during which both the atomic distribution and the magnetic configuration were free to evolve. The energetic parameters previously calculated were employed. The critical temperatures obtained with this procedure are shown in figure 7, and confronted with the experimental data.

While the temperatures for configurational order remain unaffected by the inclusion of magnetic interactions, the predicted Curie temperatures are sensitive to an incomplete degree of atomic order. This is better understood by comparing figures 2, 6 and 7. In figure 8, the thermal evolution of the *lro* parameters and magnetization in Cu$_2$AlMn is shown. Comparison with figures 3(f) and 5(a) reinforces the conclusion that the inclusion of magnetic degrees of freedom has little effect on the evolution of the atomic distribution, while an incomplete degree of chemical ordering leads to an appreciable decrement in the Curie temperatures. This situation contrasts with what is found in other alloys (e.g. Ni–Fe [48], Fe–Al [49]), in which atomic ordering and magnetism influence each other to comparable extents; the difference is that in these systems T_c is closer to (or even higher than) the critical ordering temperatures. Figure 8 also shows that, despite the considerable differences in the temperatures for atomic and magnetic ordering, the atomic equilibrium distribution at the experimental Curie temperature does not exactly correspond to a perfectly ordered lattice. Then, the values of the
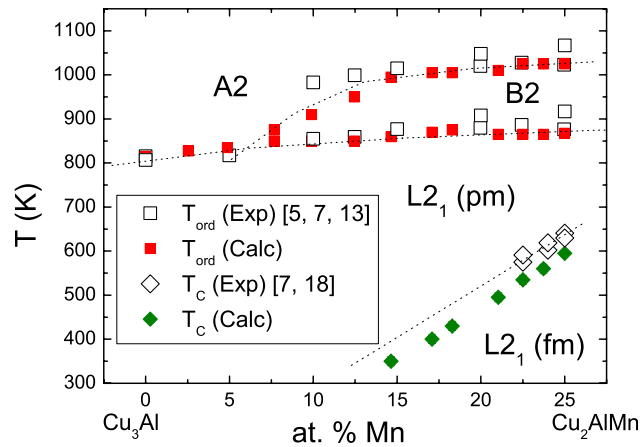
Figure 7. Critical temperatures for atomic and magnetic ordering for alloys with compositions belonging to the line $Cu_3Al \leftrightarrow Cu_2AlMn$. Lines through the experimental data are just guides for the eyes.
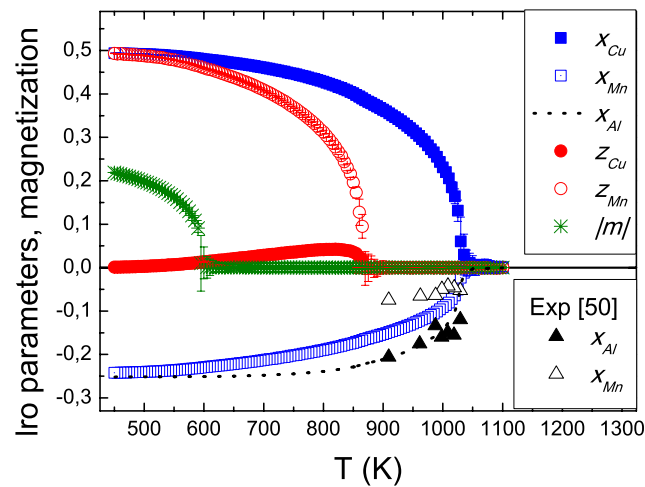

Figure 8. Thermal evolution of the configurational *lro* parameters in nearest (x_{Cu}, x_{Mn}, x_{Al}) and next-nearest (z_{Cu}, z_{Mn}) neighbours, and the modulus of magnetization ($|m|$) in Cu_2AlMn. Triangles are experimental values of x_{Al} and x_{Mn} adapted from [50].

magnetic interactions, when calculated under the assumption of perfect crystalline order, are underestimations of the actual values, and will lead to the prediction of low Curie temperatures when this restriction is removed. The magnitude of the underestimation in T_C is, according to the data displayed in figure 7, around 10%; this would be easily solved by rescaling the magnetic exchange interactions.

In figure 8, the calculated evolution of the nearest neighbours *lro* parameters below the A2–B2 transition is compared with the experimental values obtained by McCormack *et al* [50]. The calculated values favourably compare with the measured ones, although a somewhat higher thermal rate of (dis)ordering is predicted for the Mn atoms. In agreement with [50], the model predicts that, when B2 ordering is established, the (Al + Mn) sublattices (sublattices III + IV
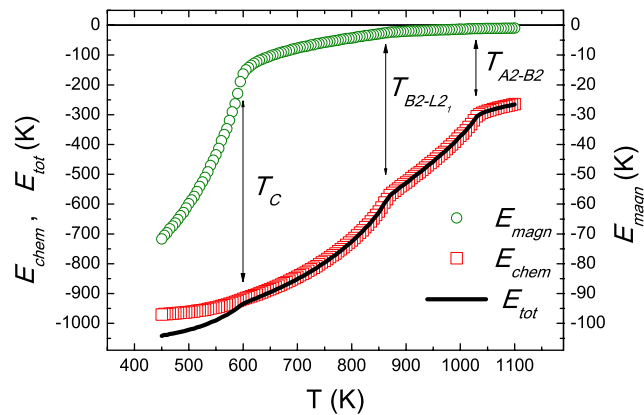
Figure 9. Thermal variation of the magnetic, chemical, and total internal energy in Cu_2AlMn.

in figure 1) are preferentially occupied by the Al atoms, at the expense of Mn. In order to clarify this point, the parameter $x_{Al} = -x_{Cu} - x_{Mn}$ is also plotted, with a dashed line, in figure 8.

The internal energy (chemical, magnetic, and total) of Cu_2AlMn is represented in figure 9. The contribution of chemical energy is roughly one order of magnitude higher than the magnetic one. The influence of magnetism on the internal energy is only noticeable below the Curie temperature. However, some short-range magnetic ordering exists above this point, as is evident from the deviation of the magnetic energy with respect to the paramagnetic state. The effects of short-range order on the chemical energy are also noticeable: above $T_{A2\leftrightarrow B2}$, there is a considerable amount of energy stored in the form of short-range correlations. Note that the internal energy does not exhibit jumps below the critical temperatures for atomic ordering: this is due to the continuous character of both transitions, as discussed in sections 3.2.1.

It is known that different magnetic properties depend on the degree of order of the Mn atoms [51–53]. For instance, the measured values for T_c in Cu_2AlMn range between 590 and 641 K [7, 18, 53, 54]; the scatter may be attributed to variations in the configurational order. Since experiments on magnetic properties are carried out under a variety of previous thermal treatments, it should be interesting to have a measure of the degree in which the lack of perfect ordering affects such properties. The predicted dependence of the Curie temperature with the degree of atomic order in Cu_2AlMn is shown in figure 10. Simulations were carried out in the following way: first, the atomic configuration of the virtual crystal was equilibrated at different temperatures T_{eq}. Then, the temperature was varied in small steps keeping the atomic distribution fixed, but allowing the modification of the magnetic state of the Mn atoms. The $T_{A2\leftrightarrow B2}$ and $T_{B2\leftrightarrow L2_1}$ temperatures are indicated with dotted vertical lines in figure 10. As expected, T_c diminishes as the amount of chemical disorder increases. For atomic distributions corresponding to equilibrium at temperatures $T_{eq} \leqslant 600$ K, the calculated Curie temperatures are in the range of the reported experimental values. Above $T_{eq} \approx 600$ K the effects of disordering become more notorious; experimental validation of these results will depend, however, on the ability to retain frozen disorder by a suitable thermal treatment.
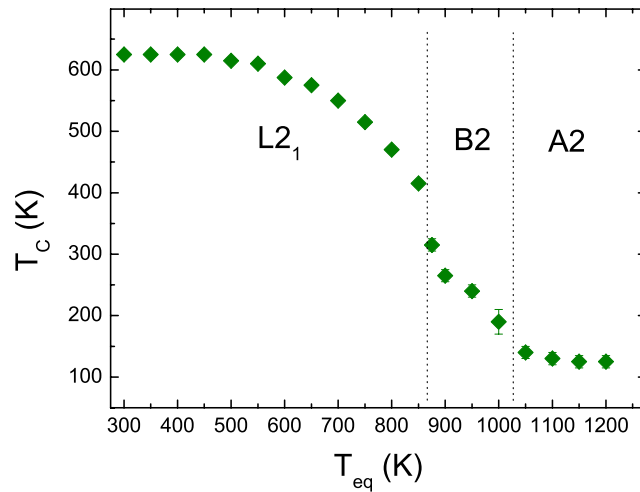
Figure 10. Dependence of the Curie temperature, T_C, with the degree of retained configurational (dis)order in Cu_2AlMn.

4. Conclusions

In summary, in this work we present a model that describes the configurational and magnetic ordering transitions taking place in β Cu–Al–Mn. The thermal evolution of the atomic and magnetic ordering degree was studied by means of Monte Carlo simulations. The simulations were based on a Hamiltonian composed of two parts: a BEG Hamiltonian to model site interchanges of neighbouring atoms, and an Ising model for the simulation of the magnetic behaviour.

A set of constant chemical interchange energies in nearest and next-nearest neighbours was calculated. These energies allow an accurate reproduction of the structure of the involved phases, critical temperatures for long-range ordering, and kinetics of the transitions for alloys with compositions along the pseudobinary line $Cu_3Al \leftrightarrow Cu_2AlMn$. For other compositions, however, the reproduction of experimental critical temperatures is not completely satisfactory: although more experimental information is necessary to draw a definitive conclusion, it seems that a dependence of the interchange energies on composition (or multi-body terms) should be included in the model.

The dependence with composition and temperature of the paramagnetic/ferromagnetic transition temperature was modelled by means of an Ising model. The model parameters (exchange integrals) were calculated by combining first principles calculations of the ground state energy for ferro and antiferromagnetic $L2_1 Cu_2AlMn$ structures, and the experimental value of the Curie temperature. The model correctly predicts the linear dependence of the Curie temperature with the Mn content.

Finally, by performing simulations with simultaneous variation of the atomic distribution and the magnetic state, the interplay between both processes was analysed. It has been shown that, whereas the atomic ordering transitions remain unaffected by the existence of magnetic interactions, the magnetic ordering is very sensitive to the degree of configurational order.

Other authors have suggested that the magnetism of an ordered alloy may give rise to a low-temperature phase separation between a ferromagnetic and a paramagnetic phase [43]. In the cited work, a model normalized Hamiltonian was employed; the model was constructed based

on the topology of the phase diagram of Cu–Al–Mn, which displays a DO_3 (paramagnetic)+$L2_1$ (ferromagnetic) two-phase field at low temperatures. However, the authors did not suggest numerical values for the chemical and magnetic interactions. The numerical values proposed in the present work would constitute a good starting point for a more detailed study of the influence of magnetism in the formation of this two-phase field.

Acknowledgments

References

[1] Delaey L, Van Humbeeck J, Chandrasekaran M, Janssen J, Andrade M and Mwamba N 1981 *Met. Forum* **4** 164–75

[2] Tadaki T 1998 Cu-based shape memory alloys *Shape Memory Materials* ed K Otsuka and C M Wayman (Cambridge: Cambridge University Press)

[3] Warlimont H and Delaey L 1974 *Prog. Mater. Sci.* **18** 1

[4] Delaey L 1991 Diffusionless transformations *Materials Science and Technology* vol 5 *Phase Transformation in Materials* ed P Haasen (Weinheim, F R Germany: VCH)

[5] Bouchard M and Thomas G 1975 *Acta Metall.* **23** 1485–500

[6] Soltys J 1981 *Phys. Status Solidi* **63** 401–6

[7] Kainuma R, Satoh N, Liu X J, Ohnuma I and Ishida K 1998 *J. Alloys Compounds* **266** 191–200

[8] Prado M, Sade M and Lovey F 1993 *Scr. Metall. Mater.* **28** 545–8

[9] Obradó E, Frontera C, Mañosa Ll and Planes A 1998 *Phys. Rev.* B **58** 14245

[10] Murray J L 1985 *Int. Met. Rev.* **30** 211–34

[11] Jurado M, Castán T, Mañosa L l, Planes A, Bassas J, Alcobé X and Morin M 1997 *Phil. Mag.* A **75** 1237–50

[12] Lanzini F, Romero R and Castro M L 2008 *Intermetallics* **16** 1090–94

[13] Lanzini F, Romero R, Stipcich M and Castro M L 2008 *Phys. Rev.* B **77** 134207

[14] Roulin G and Duval P 1997 *Scr. Mater.* **37** 45–51

[15] Lanzini F, Romero R and Stipcich M 2011 *J. Phys.: Condens. Matter* **23** 405404

[16] Ishikawa Y 1977 *Physica* B + C **91** 130–7

[17] Tashima K, Ishikawa Y, Webster P J, Stringfellow M W, Tocchetti D and Ziebeck K R A 1977 *J. Phys. Soc. Japan* **43** 483

[18] Oxley D P, Tebble R S and Williams K C 1963 *J. Appl. Phys.* **34** 1362–4

[19] Marcos J, Planes A and Mañosa Ll 2002 *Phys. Rev.* B **66** 054428

[20] Ulakko K, Huang J K, Kantner C, O´Handley R C and Kokorin V V 1996 *Appl. Phys. Lett.* **69** 1966

[21] Blume M, Emery V J and Griffiths R B 1971 *Phys. Rev.* A **4** 1071

[22] Binder K (ed) 1987 *Monte Carlo Methods in Statistical Physics* (Berlin: Springer)

[23] Mouritsen O G 1984 *Computer Studies of Phase Transitions and Critical Phenomena* (Berlin: Springer)

[24] Inden G and Pitsch W 1991 *Materials Science and Technology: A Comprehensive Treatment* vol 5 (Weinheim: VCH)

[25] Ducastelle F 1991 *Order and Phase Stability in Alloys* (Amsterdam: North-Holland)

[26] Metropolis N, Rosenbluth A W, Rosenbluth M N, Teller A H and Teller E 1953 *J. Chem. Phys.* **21** 1087

[27] Hohenberg P and Kohn W 1964 *Phys. Rev.* B **136** 864

[28] Giannozzi P *et al* 2009 *J. Phys.: Condens. Matter* **21** 395502

[29] Vanderbilt D 1990 *Phys. Rev.* B **41** 7892–95

[30] Perdew J P, Burke K and Ernzerhof M 1996 *Phys. Rev. Lett.* **77** 3865–8

[31] Monkhorst H J and Pack J D 1976 *Phys. Rev.* B **13** 5188

[32] Rapacioli R and Ahlers M 1977 *Scr. Metall.* **11** 1147

[33] Recarte V, Lambri O A, Pérez-Sáez R B, Nó M L and San Juan J 1997 *Appl. Phys. Lett.* **70** 3513–5

[34] Kainuma R, Liu X J, Ohnuma I, Hao S M and Ishida K 2005 *Intermetallics* **13** 655–61

[35] Gu Y, Jin M and Jin X 2009 *Intermetallics* **17** 704–7

[36] Inden G 1975 *Z. Metallkd.* **66** 577
Inden G 1975 *Z. Metallkd.* **66** 648

[37] Lanzini F, Romero R and Rubiolo G H 2011 *Calphad* **35** 396–402

[38] Massalski T B and Mizutani U 1978 *Prog. Mater. Sci.* **22** 151–262

[39] Hume-Rothery W 1926 *J. Inst. Met.* **35** 319–35

[40] Miettinen J 2003 *Calphad* **27** 103–14

[41] Obradó E, Vives E and Planes A 1999 *Phys. Rev.* B **59** 13901–10

[42] Vives E, Obradó E and Planes A 2000 *Physica* B **275** 45–9

[43] Marcos J, Vives E and Castán T 2001 *Phys. Rev.* B **63** 224418

[44] Ruderman M A and Kittel C 1954 *Phys. Rev.* **96** 99
Kasuya T 1956 *Prog. Theor. Phys.* **16** 45
Yosida K 1957 *Phys. Rev.* **106** 893

[45] Kübler J, Williams A R and Sommers C B 1983 *Phys. Rev.* B **28** 1745–55

[46] Ashcroft N and Mermin D 1976 *Solid State Physics* (New York: Holt. Rinehart y Winston)

[47] Moran-López J L, Rodríguez-Alba R and Aguilera-Granja F 1994 *J. Magn. Magn. Mater.* **131** 417–26

[48] Vernyhora I V, Ledue D, Patte R and Zapolsky H 2010 *J. Magn. Magn. Mater.* **322** 2465–70

[49] Schmid F and Binder K 1992 *J. Phys.: Condens. Matter* **4** 3569–88

[50] McCormack R, Asta M, Hoyt J J, Chakoumakos B C, Misture S T, Althoff J D and Johnson D D 1997 *Comput. Mater. Sci.* **8** 39–45

[51] Johnston G B and Hall E O 1968 *J. Phys. Chem. Solids* **29** 193–200

[52] Winkler R and Wachtel E 1978 *J. Magn. Magn. Mater.* **9** 270–2

[53] Kudryavtsev Y V, Oksenenko V A, Lee N N, Lee Y P, Rhee J Y and Dubowic J 2005 *J. Appl. Phys.* **97** 113903

[54] Dubois B and Chevereau D 1979 *J. Mater. Sci.* **14** 2296